Available online at www.sciencedirect.com
SCIENCE DIRECT®
International Journal of Heat and Mass Transfer 47 (2004) 4403–4414
International Journal of HEAT and MASS TRANSFER
www.elsevier.com/locate/ijhmt

Pendant droplet motion for absorption on horizontal tube banks

Jesse D. Killion, Srinivas Garimella *

George W. Woodruff School of Mechanical Engineering, Georgia Institute of Technology, Atlanta, GA 30332-0405, USA

Received 12 September 2003; received in revised form 14 April 2004

Abstract

Falling films on internally cooled horizontal tube banks are widely used in the absorbers of absorption heat pumps. Recent literature suggests that the droplets that form on the underside of the tubes play a large part in the absorption process. Flow visualization of aqueous lithium–bromide solutions falling over 15.9 mm OD tubes using high-speed video is presented here. The results illustrate the characteristic droplet evolution pattern, including the axial elongation along the tube, the formation of a primary droplet, trailing liquid thread, and satellite droplets, and the formation of saddle waves due to the spreading lamellae of the primary droplet impacts. In addition, a new image analysis method is developed to quantify the surface area and volume of the droplets during their formation, detachment, fall and impact. Using a semi-automated edge-detection process, a mathematical description of the interface of the droplets is generated for each frame of a sequence. The results show that the surface area and volume of a droplet between the tubes increase until the primary droplet impacts the tube beneath. The surface area and volume both drop sharply after impact as the main liquid inventory of the droplet joins the film surrounding the tube. As the trailing liquid thread breaks into satellite droplets, the surface-area-to-volume ratio reaches a maximum. These results are useful for developing more realistic models of heat and mass transfer in droplets pendant from horizontal tubes.

1. Introduction

Internally cooled horizontal tube banks over which a liquid film falls due to gravity are used in many applications, in particular in the absorbers of absorption heat pumps. The heat and mass transfer occurring across the film is affected by the details of the flow pattern of the liquid film. In most absorption heat pumps, the liquid flow rate is such that droplets form on the bottom of each tube and fall onto the top of the tube beneath. It has been suggested in the literature that a significant portion of the total absorption occurs on the pendant liquid droplets [1–5]. In addition, the behavior of the droplets affects the waviness and temporal distribution of the liquid film surrounding the tubes. Thus, understanding the behavior of the droplets is important for the understanding of the overall absorption process on falling films over horizontal tubes. In most models of absorption on horizontal tubes, the effects of droplets are essentially neglected: the film is assumed to be smooth, uniformly distributed, and instantly transported from the bottom of one tube to the top of the next without the possibility of absorption [6–8]. Previous models of the absorption process on horizontal tubes that have separately considered the role of droplets have been forced to utilize greatly simplified assumptions about the shape of the droplets during formation and fall (as well as oversimplifying the effects of droplet impact) [2,3]. The evolution of the shape of droplets forming in horizontal tube banks with falling water films has been investigated using high-speed digital photography [5]. This analysis revealed that the flow pattern differed significantly from the idealized pattern often

* Corresponding author.
E-mail address: srinivas.garimella@me.gatech.edu (S. Garimella).

0017-9310/$ - see front matter © 2004 Elsevier Ltd. All rights reserved.
doi:10.1016/j.ijheatmasstransfer.2004.04.032

Nomenclature

A	surface area
abs	absolute value operator
d	differential operator (length, area, volume, etc.)
f, g	spline functions for x, y coordinates, respectively
r, Θ, z	cylindrical coordinates
s	arc-length
t	parameter for spline function, roughly equivalent to arc-length
V	volume
x, y, z	Cartesian coordinates

Sub/superscripts

A	axis of rotation
$'$	differential with respect to t

assumed in the literature. The progression of events that characterizes the evolution of droplets in these systems was shown for the case of water falling over a horizontal tube bank with 12.7 mm outside-diameter tubes spaced 25.4 mm apart. The present work extends this analysis to the case of aqueous lithium–bromide solutions, a working fluid pair encountered frequently in absorption heat pumps, falling over a bank of horizontal 15.9 mm diameter tubes spaced 15.9 mm apart, a geometry characteristic of absorber designs used in commercial absorption heat pumps. In addition, a new method for analyzing the shape of the droplet interface is developed, which allows the quantification of droplet surface area and volume during the evolution of a pendant drop. This is accomplished by developing a mathematical description for the coordinates of the interface contained in each of a sequence of high-speed video. This mathematical description is a piecewise-smooth spline function that uniquely minimizes the surface area of the function given the coordinates identified on the droplet interface. Using a known reference dimension from the video, this function can be appropriately integrated to estimate the temporal development of droplet surface area and volume during droplet formation and detachment. This information provides valuable insight and information for accurately modeling the transport processes on pendant droplets.

2. Previous studies

The phenomenon of droplet formation has been studied for hundreds of years. According to the review by Eggers [9], droplet formation was first mentioned in scientific literature in 1686 by Mariotte [10]. Investigating the formation of droplets from fluid jets, Savart in 1833 [11], Plateau in 1849 [12], and the famous works of Rayleigh in 1879 [13,14] laid much of the foundation for modern understanding of the formation of droplets. In 1908, Worthington published "A Study of Splashes" which contains 197 remarkable photographs of the coronet splashes that occur when droplets or solids fall onto films or into pools [15]. Work in this field continues today aided by the advent of high performance computers and high-speed, high-resolution video cameras. In addition, due to the inherent natural beauty of droplet formation, the phenomenon has made forays into popular culture with works like the famous milk-drop splash of Edgerton [16] (see Fig. 1a) and many print and television advertisements. Many empirical/modeling tech-

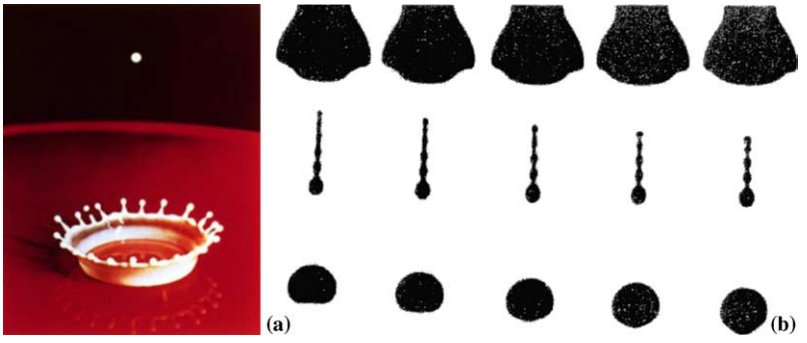

Fig. 1. (a) Famous milk-splash coronet photo [16], copyright (2004) Harold & Esther Edgerton Foundation, reprinted with permission courtesy of Palm Press Inc. (b) Example photograph from Hauser, Edgerton et al. [24], reprinted with permission from *Journal of Physical Chemistry*, copyright (1936) American Chemical Society.

niques have been developed as a result of experimental investigations into the problem of droplet formation. Some of these are summarized by Kumar and Kuloor [17], Clift et al. [18] and Frohn and Roth [19]. A recent review by Eggers [9] provides an excellent summary of many modern mathematical, experimental, and computational methods utilized to better understand the details of the droplet behavior. Eggers directs particular attention to the case of droplets forming from jets or capillary tubes and the dynamics of the bifurcation event. Other reviews covering similar topics can be found in [20–22].

The above review of the literature shows that *axisymmetric* cases have received the vast majority of the attention. The case of *formation under horizontal tubes*, however, leads to significant differences from most of the literature in terms of the overall shape, size, and internal velocity fields of the droplets, especially in the early stages of droplet formation where the extent of the droplet in the lengthwise direction of the tube may be several times its extent in the circumferential direction. In the latter stages of development, the droplets assume axisymmetric shapes; however, the size and motion during this period has been determined by the influence of the 3-D structures of the tubes. In addition, the likelihood of the behavior of one droplet to influence a nearby droplet via impact and film waviness is high in the case of tube banks, especially as the flow rate is increased. The possibility of this type of interaction does not exist in droplet formation from capillary tubes or liquid jets. Also, interactions between droplets in sprays, which have received considerable attention, are governed by completely different mechanisms than those under consideration here.

The early works of Edgerton and coworkers [23,24] are some of the first to experimentally show the development of droplets from capillary tubes. The shadowgraphs and photographs presented show some of the features of the formation and detachment process for several fluids including water and glycerin and alcohol. These pictures have enough resolution to show that satellite droplets form from the collapse of the liquid bridge between the primary drop and the parent fluid after the bridge breaks from each attachment point (see Fig. 1b). Also, the effects of thermophysical properties, including viscosity and surface tension, on the length, diameter, and stability of the drops and bridge are illustrated. The authors note that "the secondary drop in most cases vibrates very violently and at first somewhat irregularly." At a low flow rate, a pendant drop essentially assumes a series of equilibrium shapes until the surface tension can no longer support the weight of the drop; equilibrium droplet shape and stability have been considered in the literature [9,22,25,26]. Even at exceedingly low flow rate, the events occurring near the final pinch point or bifurcation proceed at time and length scales that depend almost entirely on fluid properties [9,27]. Peregrine et al. [27] are perhaps the first to present (and note the self-similarity of) the characteristics of the bifurcation of droplet detachment in enough detail to resolve some of the motion at these very short length and time scales. They present very vivid, magnified photographs of the times before, after, and near the instant of bifurcation for a droplet of water emerging from a 5.2 mm capillary tube. Many of the features described by Edgerton, Peregrine and their coworkers are also exhibited with droplets forming under horizontal tubes: necking and the formation of a thinning liquid bridge or thread between the droplet and the parent liquid above it, a conical point attached to the nearly spherical droplet at the instant of bifurcation, the fast recoil and instabilities exhibited by the broken liquid bridge, and a secondary bifurcation at the opposite end of the liquid bridge leading to the formation of satellite droplets. de Bruyn [28] studied the formation of droplets on very small cylinders (11 μm to 1.27 cm) initially coated with a uniform film of various viscous liquids to investigate the transition from surface-tension-driven instabilities (Rayleigh) to gravity-driven instabilities (Rayleigh–Taylor). He also observed some of these same phenomena on the droplets formed from the larger tubes although with much lower resolution.

The impact of droplets in the case of horizontal tubes and falling films has not received a great deal of attention. However, droplet impact in general is a field that is widely studied. Rein [29] has provided a good review of impacts on dry walls and liquid pools. Tropea and Marengo [30] have also reviewed the impact of droplets on walls and films. In an entertaining and informative review, Prosperetti and Oğuz [31] have summarized the impact of liquid drops onto liquid surfaces with the objective of understanding the characteristics of sound generated underwater by rain; the results are useful for determining rainfall amounts over large bodies of water. The bulk of the studies can be divided into two groups: impact of droplets onto dry surfaces and impact of droplets into liquid pools. The case of impact onto thin films has received considerably less attention and when studied, the film thicknesses used are generally of the order of the drop size; much thicker than the films considered here. Rein [29] suggests that in the limit of thin films, "the events become in many respects similar to splashing on solid walls". Furthermore, Levin and Hobbs [32] report that, in terms of splashing, there is little difference between a dry surface and a wet one except that the time scales are shorter for the wet surface. Weiss and Yarin [33] showed that if surface tension is sufficiently high and/or impact speed low enough to suppress the formation of a crown and thus the possibility of splashing, then their numerical results for impact of droplets onto thin films were similar to those of researchers who had considered dry surfaces. Yarin and

Weiss [34] investigate the capillary waves that form during droplet spreading and the transition to splashing when droplets impact a flat surface with a thin liquid film. There are key differences between the two situations. For a dry wall impact, the roughness of the surface and the dynamic (advancing and retreating) contact angle (dependent on the relationship between the surface tension in the three phases [35]) have a strong effect on the splashing and spreading behavior [29,30,36,37]. In fact Stow and Hadfeild [38] suggest that the splashing threshold depends more strongly upon surface roughness the smoother the surface is. Many researchers [30,39–41] have shown also that the presence and depth of a shallow liquid layer has a great influence on the outcome of splashing. Rein [29] and Mundo et al. [42] provide several methods for estimating the conditions required for the onset of splashing. Although the limits do not completely agree with each other, for the parameters of the current study, they all suggest that splashing would not occur, which agrees with what is observed below.

When droplet impact leads to spreading without splashing, the thin film formed that propagates away from the point of impact with a decreasing velocity is called a lamella [29]. It has been noted in the literature that the leading edge of the lamella is generally thickest. The behavior of the lamella leads to another difference between the current case and that of impact on a dry surface. In the case of impact on a dry surface, the lamellae often expand to a maximum diameter and then retract, owing to surface tension, to an equilibrium shape. In contrast, with a wet surface, the lamellae expand until they are no longer distinguishable features. In the case of impact onto a horizontal tube covered with a thin film, the geometry is not axisymmetric due to the preferential downward flow resulting from gravity, and the spreading lamella is no longer circular. A characteristic "saddle" shape develops, as will be seen below. Thus in addition to the fact that impact on thin films without splashing has been studied less, it is difficult to directly compare the results found in literature with the present 3-D (non-axisymmetric) case.

3. Experimental setup

The bank of horizontal tubes used in the present study was a single column of nine copper tubes 15.9 mm in diameter and approximately 500 mm long. With the primary focus being an understanding of fluid flow, the apparatus did not include any provision for absorption or heat transfer. The tube center-to-center spacing was 31.8 mm, providing a 15.9 mm tube-to-tube distance. The fluid used was surfactant-free aqueous lithium–bromide (53.44% LiBr by weight, see Table 1 for a summary of thermophysical properties) and the whole apparatus was surrounded by air at atmospheric pressure. A pump was used to circulate the liquid first through a rotameter, which both controlled and measured the flow rate, then into the distributor. The distributor was designed to promote even distribution of liquid along its length (500 mm). To accomplish this, 16 evenly spaced small holes were introduced along a 15.9 mm OD tube and oriented such that the solution flowed upward through them (a in Fig. 2). The high-velocity flow through these holes impinged on the inside of a 17.7 mm ID surrounding outer tube, the bottom half of which was cut away. The liquid then flowed through the partial annulus between the tubes and formed droplets on the underside of the inner tube. The high-velocity

Table 1
Summary of properties at 25 °C

	Water	53.4 wt.% LiBr
Density (kg/m^3)	997	1564
Viscosity (kg/m s)	8.9×10^{-4}	4.1×10^{-3}
Surface tension (N/m)	7.3×10^{-2}	9.1×10^{-2}

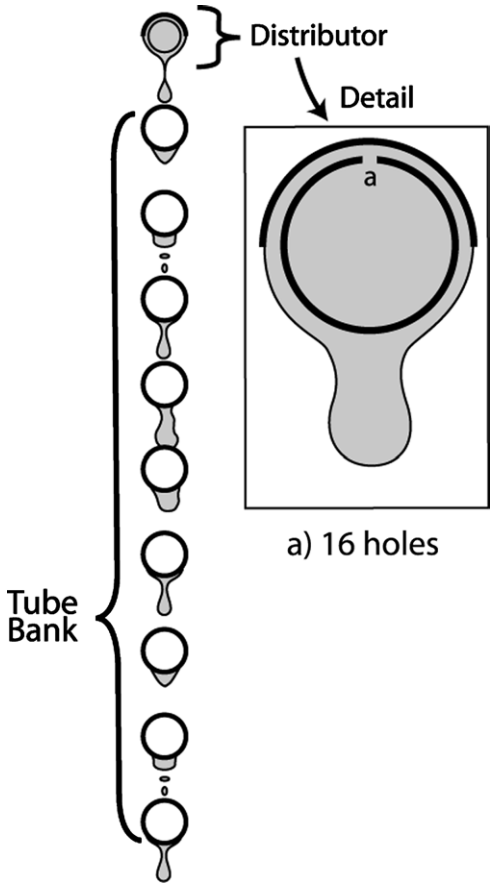

Fig. 2. Schematic of tube bank.

flow through the small holes ensured equal distribution along the length of the tube (no header effects), but the configuration of the header ensured the flow pattern on the top tube was similar to that on every subsequent tube in the column. Flow rates could be increased to the point that liquid columns would form, which aided in establishing complete wetting on the tubes at the commencement of testing, but for most of the testing, the flow rate was kept much lower than this to generate droplet flow between the tubes. Before testing, the tube surfaces were thoroughly cleaned.

The high-speed digital video camera used to capture the images of the film, made by Photron [43], had a resolution of 1024×1024 at 500 frames per second. The camera was computer controlled through an IEEE 1394 connection and was equipped with enough memory to store 1 s of video (enough for several droplet evolution cycles to complete). The images were stored on the computer as uncompressed, color video files in the so-called AVI format. A 500 W tungsten/halogen bulb with an illumination temperature of 3200 K was used with a parabolic reflector to provide the high illumination power required for the high frame-rate and shutter-speeds used.

4. Progression of the interface

The departure of the flow patterns from the idealized patterns assumed in the literature was described in detail by Killion and Garimella [5] for water. The flow patterns with aqueous LiBr exhibit similar characteristics. Fig. 3 shows the typical evolution of a droplet from the early formation through detachment and subsequent impact on the tube below. The early formation is the result of film instabilities but is often driven or accelerated substantially by the arrival of a supply of liquid from a prior droplet impact event above the formation site. During the early formation, the droplet is stretched in the direction of the axis of the tube (Fig. 3, frames a–e). This is due to the shape of the underside of the tube and the fact that surface-tension forces are always directed tangentially to the interface surface. Thus in the axial direction, surface-tension forces tend to elongate the forming droplet, whereas those in the circumferential direction tend to pull in a more upward direction. As the droplet gains volume, the head of the droplet begins to pull away from the tube and approaches the shape of a spherical cap, which is axisymmetric with respect to a vertical axis. It appears that the droplet draws fluid from a length of the tube several times as long as the diameter of the head of the droplet. As the weight of the droplet increases, a liquid trail or thread forms that connects the primary droplet with the parent liquid above (frames k–m). This liquid thread begins to stretch and thin as the droplet accelerates downward faster than the incoming liquid can fill the thread. In the previous study with water [5], this liquid thread was stretched longer and thinner before droplet impact because the tube spacing was larger, and as a consequence, could detach at the time of, or even slightly before, droplet impact. In the present study, the thread is generally still attached to the primary droplet when the droplet impacts the tube underneath. Upon impact, the primary droplet forms a spreading saddle-shaped lamella with velocity components in the axial and circumferential directions. The

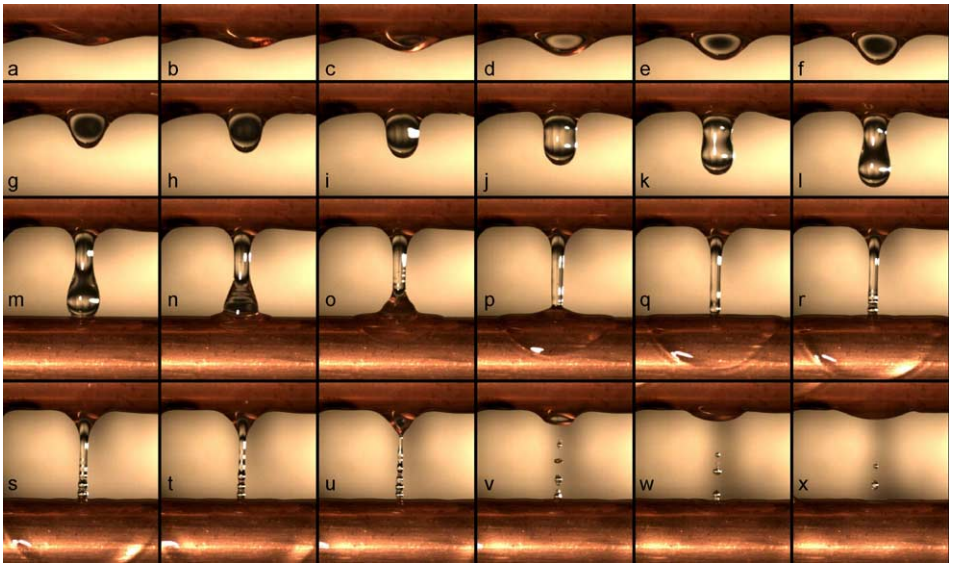

Fig. 3. Evolution of pendant drop of aqueous LiBr (a–m: 10 ms between frames, m–x: 6 ms between frames).

impulse is seen to propagate back up through the primary droplet (frame n) and into the attached liquid thread (frame o). The advancing front of the spreading liquid lamella forms a thicker wave with small capillary waves preceding it on the existing film (frames q–s). The film behind the advancing front is relatively smooth, although it is quickly thinning and spreading, flowing outward from the point of impact. The liquid thread may persist for a significant amount of time after the impact and continues to thin (frames o–t) until it eventually breaks into a number of satellite droplets (frames u–x). The bifurcation of the liquid thread is described by singularities in the equations of motion of the fluid [9] and extremely high velocities. The radius of curvature at the point of bifurcation approaches 0, which suggests that the resulting internal pressure due to surface tension is extremely high. This imbalance leads to fast recoil of the broken liquid thread. The result is that the satellite droplets may have significant shape oscillations and/or velocity after the break. Impact between the satellite droplets, between the satellite droplets and the parent liquid, or between the satellite droplets and the tube underneath can lead to bouncing or complete or partial coalescence.

5. Image analysis

The qualitative description above reveals the significant differences between the actual behavior of the droplets and what is often assumed when attempting to model the role of droplets in the absorption process. The droplets rarely, if ever, resemble a sphere or spherical section, and it is clear that the liquid thread and satellite droplets are a significant aspect of the overall process. In addition, the impact and spreading of the droplets generates a non-uniform liquid distribution along the length of the tube as well as significant velocity in the direction of the tube axis. To develop a more quantitative understanding of the behavior of the droplets, a method for mathematically analyzing the video was developed. In a semi-automated process, a mathematical description of the shape (edges) of the droplets is generated throughout their evolution. The identified interface shapes are highlighted in Fig. 5 for a selected number of frames. The mathematical description of the interface is then used to evaluate the surface area and volume of the droplets. This information is valuable for modeling the absorption on the droplets as well as for validating computation models of droplet behavior [44]. A description of the analysis technique follows.

The digital information stored from the camera contains virtually no explicit information about the motion of the droplets. The first step in the analysis, consequently, is to identify the location of the droplet interface in each frame of the video. The second step is to generate a mathematical description of the interface that is physically reasonable. The final step is to use that mathematical description to assess quantities of interest such as the surface area and volume of the droplets versus time.

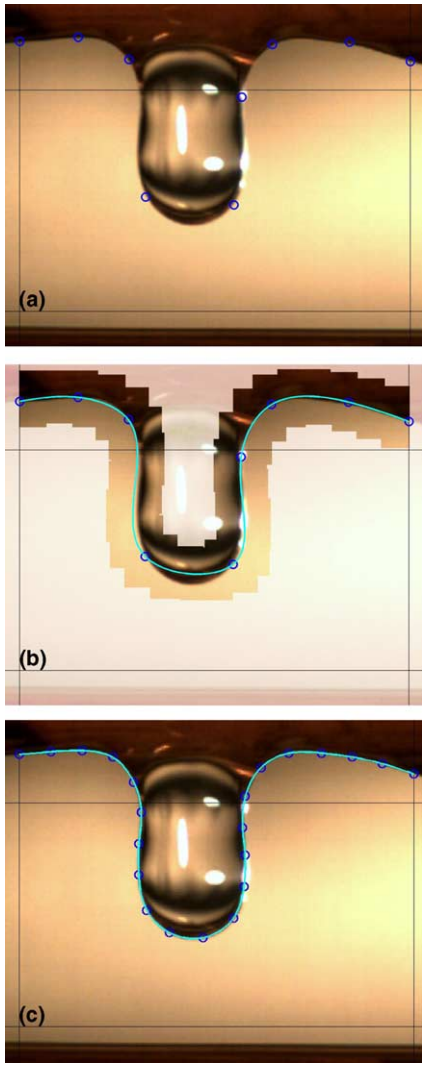

Fig. 4. Steps in image analysis: (a) identification of interface location by human eye, (b) ROI defined (highlighted), and (c) interface detected and spline fit.

Identification of the interface requires intelligent edge detection. Edge-detection algorithms are essentially 2-D filters that are used to calculate local gradients in the image, typically gradients of the image intensity [45]. The gradient operation typically accentuates high-frequency pixel noise, so most edge-detection algorithms include a Gaussian smoothing filter. Due to the lighting and nature of the system being studied, shadows and glare (highlights) as well as natural gradients in the color

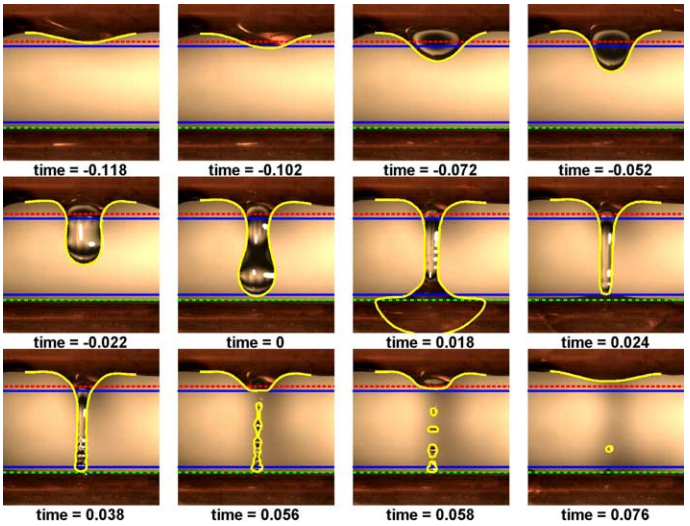

Fig. 5. Superposition of video frames and analyzed interfaces for LiBr droplet.

occur throughout the images. Thus, it is unlikely that any single edge-detection algorithm is suitable for analyzing all regions of all frames. On the other hand, it is very easy for the human eye to detect the edge of the droplet in any frame. Thus the algorithm developed is semi-automated: initially the approximate location and shape of the interface (edge of interest) is identified by eye (see Fig. 4). This information is then used to guide the interface identification program on the initial and each subsequent frame. Moreover, the edge-detection algorithms and associated threshold parameters can be adjusted as necessary for each frame to address the changing glares and shadows. A detailed description of the program developed to accomplish this is given in [4]. A graphical user interface (GUI) was developed in the commercially available software program Matlab [46]. The GUI facilitates the limited human interaction required to guide the program through the evolution of a droplet. A brief description of the program is provided next.

The GUI displays the frame to be analyzed (zoom limits and frames can be selected by appropriate controls in the GUI). On the first frame of the sequence to be analyzed, a region of interest (ROI) that includes the droplet interface is defined with a series of mouse-clicks by the user (see Fig. 4a and b). This is how high-level knowledge about the expected shape of the interface is communicated to the analysis program. An edge-detection algorithm, for instance the Canny [47] or Sobel [48] method, is selected along with the various edge intensity thresholds. The image is then analyzed and pixels that are within the defined ROI and identified by the algorithm to be an edge are highlighted. If the highlighted pixels do not conform to the actual interface, a different edge-detection algorithm can be selected, thresholds adjusted, or the ROI redefined to exclude confounding features. After the first frame, the ROI for each subsequent frame is defined based on the identified edge in the previous frame. That is, a region surrounding the identified edge in the previous frame is taken to be the ROI for the current frame. This allows many consecutive frames to be analyzed with very little human intervention, primarily at the beginning of the process. If the change in location of the interface is large from frame to frame, the ROI width can be increased or a new ROI can be manually defined as necessary. Once the edge is suitably identified, the second step is to generate an adequate mathematical description. This is accomplished using the image coordinates of a selected number of the identified edge pixels and cubic spline approximation.

Splines have gained popularity in recent years because of their powerful ability to approximate discrete data with smooth mathematical functions. In particular, splines are piecewise-polynomial functions that blend smoothly and can be efficiently stored (as coefficient arrays) and manipulated on computers. Spline functions can be created to *interpolate* between points (the function will pass precisely through the data points), smoothly *approximate* data (minimizing the second derivative while approximating the data to within a set tolerance), define a least-squares fit of arbitrary order, approximate the solution of ordinary differential equations, and more. The order, smoothness, end-conditions and various other parameters can all be controlled. For a detailed exposition of the development and practical application of splines, see [49]. Cohen et al. [50] give an introduction to techniques for modeling geometry with splines including some aspects of differential geometry. The algorithms presented by de Boor [49] have been

extended to handle vector-valued splines in the Matlab Spline Toolbox [51], which was used in this work. The primary motivation for using splines in this case is to develop appropriate and tractable mathematical representations for the positions of the liquid–vapor interface in a sequence of images. It is important to note that cubic smoothing splines have the "smoothest interpolation property" [49, p. 66], that is, they *uniquely* minimize (approximately) the strain energy for a function passing through a given set of data within the specified tolerance. Since systems having free surfaces with interfacial tension tend toward equilibrium states that minimize the surface energy, i.e. surface area [35, p. 29], splines are uniquely suited for describing the shape of the interfaces of such systems. Thus, given a finite set of coordinates defining the position of the interface that inherently contain some noise or uncertainty as any measured data must, the cubic smoothing spline is the "natural" choice for developing a continuous, mathematical definition of the interface. The two-valued (x and y coordinates) cubic smoothing splines thus used are fit through a number of the identified edge pixels and parameterized by the distance between the selected edge points, completing the second step of the analysis.

In the final step, the mathematical descriptions obtained are used to determine quantities of interest, in this case, surface area and volume. Since the images are 2D and only one camera is used, information about the thickness of dimensions in the line of sight is unavailable. However, in the regions between the tubes, the droplet shape becomes axisymmetric and so the 2-D interface can be treated as a surface of revolution. The vertical extent of the regions of axial symmetry is determined visually and by interpreting the results of the analysis, which will be discussed below. The horizontal position of the axis of revolution is taken to be the geometric average of the interface profile. Because the edge is defined on two sides of this axis of revolution, it provides two surfaces of revolution. Thus revolving the entire interface and dividing by two results in an estimate that is the average of two interface descriptions. The spline functions, $F(t)$, return x and y coordinates as a function of the parameter t, the distance between the selected interface coordinates (which is approximately the arc-length of the spline), i.e. $F(t) = (f(t), g(t)) = (x(t), y(t))$. The corresponding r and z coordinates of a cylindrical coordinate system are obtained using the following transformations:

$$z(t) = y(t) \tag{1}$$

$$r(t) = \mathrm{abs}(x(t) - x_{\mathrm{A}}) \tag{2}$$

where x_{A} is the x-coordinate of the axis of revolution (assumed to be vertical). Simple differential geometry gives the following relations for surface area and volume:

Table 2
Validation of surface area and volume calculations for a sphere with radius = 100

	Exact	Calculated	Error
Surface area	1.2566×10^5	1.2558×10^5	−0.0657%
Volume	4.1888×10^6	4.1846×10^6	−0.1004%

$$\mathrm{d}A = r\,\mathrm{d}s\,\mathrm{d}\Theta \tag{3}$$

where $\mathrm{d}s$ is the arc-length for a differential horizontal slice of height $\mathrm{d}z$.

$$\mathrm{d}V = r\,\mathrm{d}r\,\mathrm{d}\Theta\,\mathrm{d}z \tag{4}$$

Since axial symmetry is assumed, the integration with respect to $\mathrm{d}\Theta$ can be performed independently resulting in 2π. In Eq. (4), the integration of $r\,\mathrm{d}r$ can also be performed giving $r^2/2$. The arc length is defined as:

$$\mathrm{d}s = \sqrt{(\mathrm{d}r)^2 + (\mathrm{d}z)^2} \tag{5}$$

The differential lengths $\mathrm{d}r$ and $\mathrm{d}z$ are evaluated from the functional definition of the spline (a polynomial) and the transformations given in Eqs. (1) and (2). Thus in terms of the spline functions, $F(t) = (f(t), g(t))$ the integrals that must be evaluated to obtain surface area and volume are as follows:

$$A = 2\pi \int_0^{t_{\max}} \mathrm{abs}(f - x_{\mathrm{A}}) \sqrt{(f')^2 + (g')^2}\,\mathrm{d}t \tag{6}$$

$$V = \pi \int_0^{t_{\max}} \mathrm{abs}(f - x_{\mathrm{A}})(f - x_{\mathrm{A}})g'\,\mathrm{d}t \tag{7}$$

where the primes, $'$, denote differentiation with respect to the parameter, t, which starts at 0 at one end of the interface and reaches $t_{\max}$ at the other end. In Eq. (7) the absolute value only operates on one of the $r = (f - x_{\mathrm{A}})$ terms in the r^2 term. This is because the sign of g' and $(f - x_{\mathrm{A}})$ both switch as the spline goes from one side of the droplet to the other (crossing the axis of symmetry). Thus the integral is additive over the entire range. The integrals are evaluated numerically using an adaptive Simpson quadrature technique that takes advantage of the functional form of the splines to attain high accuracy [52]. The method was validated using a spline fit to 20 points on the surface of a sphere. The results tabulated in Table 2 show that the method works very accurately. Finally, the values are converted from image coordinates to SI units by calibrating the image using a dimension of known size within the image, such as the tube diameter.

6. Results

The horizontal lines in Fig. 5 show various limits used to analyze the droplet surface area and volume

discussed below. The spline fit to the interface is shown as a light solid curve. The times are referenced to the moment of impact (actually the moment when the droplet first crosses the lower boundary) as time 0. This is because the impact event provides a convenient point of synchronization for aligning the results of several analyses. Fig. 6 shows the results of the analysis of surface area, internal volume, and surface-area-to-volume ratio for the interfaces identified in the sequence. Note that the vertical grid-lines in Fig. 6 correspond to the frames shown in Fig. 5. In addition, Fig. 6 contains the shape of the splines without the underlying image at these same times (only the analyzed region is shown). It is critical to restrict the analysis of volume and surface area to the region of axial symmetry in the image. The three curves on each plot in Fig. 6 illustrate the effect of the upper and lower limits on the analysis of surface area and volume. The solid line illustrates an analysis where the upper and lower boundaries include regions that are primarily axisymmetric; the two broken lines illustrate what happens when the limits are placed too high or too low in the image and will be discussed next. In the case where the upper boundary is too close to the upper tube, the droplet just begins to cross the upper boundary at time −0.118 s. Thus the surface area and volume curves for using this boundary (dashed line) begin to rise. In the case where the upper boundary is in the axisymmetric region (the lower of the two uppermost boundaries), the droplet crosses just before time −0.102 s, which is where the solid line begins to rise. As the droplet grows and pulls away from the tube, it can be seen that the dashed line actually undergoes a region of decreasing volume (and surface area). This is not physically reasonable and reflects the fact that at −0.072 s (Fig. 6a), the interface at the boundary too close to the top tube is wider than it is at −0.052 s (Fig. 6b). This is the result of the tube stretching the droplet in the lengthwise direction. Since this stretched profile is not axisymmetric, revolving it overestimates the surface area and volume in the drop because it overestimates the depth of the droplet in the direction of view. This suggests that the lower of the two uppermost limits is a more accurate estimate of the location at which the droplet shape becomes nearly axisymmetric; the volume calculated with this boundary is strictly increasing (solid line). It can be seen that during droplet formation and the stages where it pulls away from the tube, the volume and surface area increase to a maximum value just before impact. In reality, the volume does not truly decrease after the impact, as suggested by Fig. 6; it just leaves the region of interest and is redistributed on the tube surface. However, the lack of rotational symmetry at the impact site makes accurately quantifying the volume and surface area in this region impossible since no detailed information about the film thickness is available. The interface tracked after the impact can be forced to follow the spreading lamella (saddle wave) as shown in the profile at 0.018 s in Fig. 5. There is no particular incentive to do this other than for visual interpretation. This is because the section of the spline depicting the saddle wave

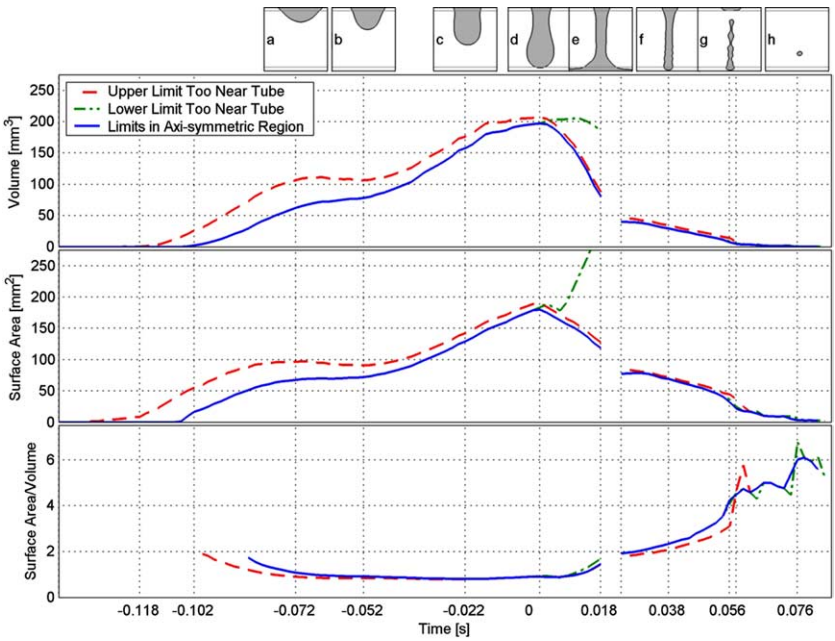

Fig. 6. Image analysis results: droplet volume, surface area, and area/volume ratio throughout the entire droplet evolution cycle.

should not be included in the calculation of surface area or volume since it is not axisymmetric and it overlaps the tube. However, the dot-dashed line (seen extending to the right of the peaks in the graphs) shows the result of continuing the analysis in this way when the lower limit is beyond the region of axial symmetry. Actually, the dot-dashed line does provide some physically reasonable insight into the spreading lamella. The calculated surface area of the droplet shoots up shortly after impact while the volume remains relatively constant. However, the spreading lamella does not, in fact, create new surface area since the tube was already wet with film before the droplet arrived; it merely recovers it with new liquid. Thus the higher of the two bottommost boundaries (solid line) provides a more sensible estimate of the change in surface area after impact (i.e. it begins to decreases sharply at impact as the free surface of the droplet rejoins the film). Tracking the saddle wave with the spline is possible for a few frames after the impact; nevertheless, at some point, the saddle wave becomes undetectable and or/expands outside of the field of view. This necessitates reinitializing the shape of the spline (redefining the ROI) at a later frame. The frame at 0.024 s illustrates the reinitialized interface shape. Because the interface at 0.024 s does not extend beyond the lower boundary, there is a slight discontinuity in the plots, represented by the gap from 0.018 to 0.024 s in the plots in Fig. 6. It is clear that the curves on either side of the gap would intersect, but the connecting curve cannot be defined without ambiguity due to the dramatically different shapes at the bottom of the identified interface profiles at 0.018 and 0.024 s. What is clear is that shortly after impact, the volume and surface area of the primary droplet is lost to the surface of the tube resulting in a steep decline in both curves. After this, the remaining liquid bridge continues to thin and drain until it breaks and forms satellites. During this process, the volume and surface area of liquid between the tubes continues to decrease, although at a slower rate than was associated with the impact of the primary drop. It is interesting to note however, that the ratio of the surface area to the volume begins to *increase* significantly and reaches a maximum with the development of satellite droplets. It can be seen that this ratio exhibits some unsteadiness during the lifespan of the satellite droplets. This is due partly to the shape oscillation of the drops, partly to the sequential impact of the satellite drops, and partly to the increased uncertainty in the calculation of droplet sizes when the whole drop occupies just a small number of pixels. The implication of the rising area to volume ratio is that, although the total surface area and volume is small, satellite drops may absorb significant amount of vapor due to the reduced resistance to heat and mass transfer. Thus, this stage should not be neglected in absorption calculations, as has been the case in most previous studies.

7. Conclusions

Droplet formation and impact is widely studied, particularly in axisymmetric cases such as formation from a jet and impact onto a flat surface. However, in the application of interest, namely the absorbers of absorption heat pumps, the droplet behavior differs from the axisymmetric case because it occurs in a bank of horizontal tubes surrounded by falling liquid films. Using high-speed, high-resolution video, the behavior of falling films of aqueous lithium–bromide over horizontal-tube banks was observed. The characteristic features of droplet formation, detachment and impact were illustrated and described. These observations suggested the limitations of the idealized flow patterns often assumed when modeling absorption on falling films over horizontal tubes. In addition, a semi-automated digital image analysis method was developed to quantitatively analyze the recorded droplet videos. By identifying the droplet interface and developing a smooth mathematical function to describe it, estimates of the progression of droplet surface area and volume during the entire evolution cycle of a droplet were obtained. This information is valuable for modeling the absorption in horizontal tube banks as well as validating computer models of droplet formation. Other observations and conclusions are given below:

- The behavior of droplets during formation and impact in horizontal-tube banks shares some common features with the axisymmetric cases of formation from a capillary tube and impact on a flat plate, namely: the development of a primary drop with axisymmetric shape and a thinning liquid bridge connecting the primary drop to the parent liquid; the spreading of a liquid lamella after impact that initially travels with a very high velocity but steadily slows; and the formation of oscillating satellite droplets when the liquid bridge breaks.
- There are significant differences from the axisymmetric cases as well, namely: horizontal tubes elongate the droplets in the direction of the tube axis, particularly early in the formation process; lamella spreading is distorted around the tube to form a saddle-wave; and the interaction of neighboring droplets can have a sizeable impact on the details of the behavior of each drop.
- The assumption that films are evenly distributed along the top surface of a tube does not hold in the case of droplet flow where the liquid arrives at the top of the tube in discrete drops. Additionally, the momentum of an impacting drop propels a significant amount of liquid around to the underside of the tube very quickly where it may affect subsequent droplet formation events. The energy of droplet

impact also leads to waviness of the liquid film and significant axial velocity of the film.
- During pendant droplet formation and during the stages where the primary drop pulls away from the tube and a thinning liquid bridge is formed, the surface area and volume of liquid between the tubes steadily increase to a maximum the moment before impact.
- Upon impact, the surface area and volume of liquid between the tubes decreases quickly as the primary droplet is spread over the tube.
- Thinning liquid bridges exhibit a decreasing surface area and volume during their lifespan but an increasing surface-area-to-volume ratio. The maximum area-to-volume ratio occurs when the bridge breaks into satellite droplets.

Acknowledgements

The authors gratefully acknowledge the support of the National Science Foundation through grant number 9875010, ASHRAE through a Grant-in-Aid, and John Dickerson, Noah Hughes and Matt Bradshaw of Engineering Computing Support Services at Iowa State University.

References

[1] T. Nomura, N. Nishimura, S. Wei, S. Yamaguchi, R. Kawakami, Heat and mass transfer mechanism in the absorber of water/LiBr conventional absorption refrigerator: experimental examination by visualized model, in: International Absorption Heat Pump Conference, New Orleans, LA, vol. AES-31, The Advanced Energy Systems Division, ASME, 1993, pp. 203–208.
[2] M.J. Kirby, H. Perez-Blanco, A design model for horizontal tube water/lithium bromide absorbers, ASME Heat Pump Refrig. Syst. Des., Anal. Appl. 32 (1994) 1–10.
[3] S. Jeong, S. Garimella, Falling-film and droplet mode heat and mass transfer in a horizontal tube LiBr/water absorber, Int. J. Heat Mass Transfer 45 (7) (2002) 1445–1458.
[4] J.D. Killion, S. Garimella, A review of experimental investigations of absorption of water vapor in liquid films falling over horizontal tubes, HVAC&R Res. 9 (2) (2003) 111–136.
[5] J.D. Killion, S. Garimella, Gravity-driven flow of liquid films and droplets in horizontal tube banks, Int. J. Refrig. 26 (5) (2003) 516–526.
[6] J.W. Andberg, G.C. Vliet, Absorption of vapors into liquid films flowing over cooled horizontal tubes, in: Second ASME-JSME Thermal Engineering Joint Conference, Honolulu, Hawaii, vol. 2, 1987, pp. 533–541.
[7] S.K. Choudhury, A. Nishiguchi, D. Hisajima, T. Fukushima, T. Ohuchi, S. Sakaguchi, Absorption of vapors into liquid films flowing over cooled horizontal tubes, in: Proceedings of the 1993 Annual Meeting of the American Society of Heating, Refrigerating and Air-Conditioning Engineers, Inc., Denver, CO, USA, June 27–30, 1993, vol. 99, ASHRAE, Atlanta, GA, USA, 1993, pp. 81–89.
[8] Z. Lu, D. Li, S. Li, B. Yu-Chi, A semi-empirical model of the falling film absorption outside horizontal tubes, in: International Ab-Sorption Heat Pump Conference, vol. 2, 1996, pp. 473–480.
[9] J. Eggers, Nonlinear dynamics and breakup of free-surface flows, Rev. Mod. Phys. 69 (3) (1997) 865–929.
[10] E. Mariotte, Traite' Du Mouvement Des Eaux Et Des Autres Corps Fluids, E. Michallet, Paris, 1686.
[11] F. Savart, Memoire sur la Constitution des Veines Liquides Lancees par des Orifices Circulaires en Mince Paroi, Annal. Chim. 53 (1833) 337–386 (with additional plates in vol. 54).
[12] J. Plateau, Acad. Sci. Bruxelles. Mem. 23 (5) (1849).
[13] L.J.W.S. Rayleigh, On the instability of jets, Proc. London Math. Soc. 10 (1879) 4–13.
[14] L.J.W.S. Rayleigh, On the capillary phenomena of jets, Proc. Roy. Soc. London: A 29 (1879) 71–97.
[15] A.M. Worthington, A Study of Splashes, Longmans Green and Co, London, 1908, p. xii, 129, 1 l.
[16] H.E. Edgerton, 1957. Milk Drop Coronet, Cambridge, MA. Available from <http://web.mit.edu/museum/exhibits/flashes5.html>.
[17] R. Kumar, N.R. Kuloor, The formation of bubbles and drops, Adv. Chem. Eng. 8 (1970) 255–368.
[18] R. Clift, J.R. Grace, M.E. Weber, Bubbles, Drops, and Particles, Academic Press, New York, 1978, p. 380.
[19] A. Frohn, N. Roth, Dynamics of Droplets, in Experimental Fluid Mechanics, Springer, New York, 2000, p. 292.
[20] D.B. Bogy, Drop formation in a circular liquid jet, Ann. Rev. Fluid Mech. 11 (1979) 207–228.
[21] A.L. Yarin, Free Liquid Jets and Films: Hydrodynamics and Rheology, Longman Publishing Group, 1993.
[22] S. Middleman, Modeling Axisymmetric Flows: Dynamics of Films, Jets, and Drops, Academic Press, San Diego, 1995, p. 299.
[23] H.E. Edgerton, E.A. Hauser, W.B. Tucker, Studies in drop formation as revealed by the high-speed motion camera, J. Phys. Chem. 41 (1937) 1017–1028.
[24] E.A. Hauser, H.E. Edgerton, B.M. Holt, J.T. Cox Jr., The application of the high-speed motion picture camera to research on the surface tension of liquids, J. Phys. Chem. 40 (1936) 973–988.
[25] A.M. Worthington, On pendent drops, Proc. Roy. Soc. London 32 (1881) 362–377.
[26] E. Pitts, The stability of pendant liquid drops. Part 2. Axial symmetry, J. Fluid Mech. 63 (1974) 487–508.
[27] D.H. Peregrine, G. Shoker, A. Symon, The bifurcation of liquid bridges, J. Fluid Mech. 212 (1990) 25–39.
[28] J.R. de Bruyn, Crossover between surface tension and gravity-driven instabilities of a thin fluid layer on a horizontal cylinder, Phys. Fluids 9 (6) (1997) 1599–1605.
[29] M. Rein, Phenomena of liquid drop impact on solid and liquid surfaces, Fluid Dyn. Res. 12 (2) (1993) 61–93.
[30] C. Tropea, M. Marengo, Impact of drops on walls and films, Multiphase Sci. Technol. 11 (1) (1999) 19–36.
[31] A. Prosperetti, H.N. Oğuz, Impact of drops on liquid surfaces and the underwater noise of rain, Ann. Rev. Fluid Mech. 25 (1993) 577–602.

[32] Z. Levin, P.V. Hobbs, Splashing of water drops on solid and wetted surfaces, hydrodynamics and charge separation, Philos. Trans. Roy. Soc. London Ser. A. Math. Phys. Sci. 269 (1200) (1971) 555–585.
[33] D.A. Weiss, A.L. Yarin, Single drop impact onto liquid films: neck distortion, jetting, tiny bubble entrainment and crown formation, J. Fluid Mech. 385 (1999) 229–254.
[34] A.L. Yarin, D.A. Weiss, Impact of drops on solid surfaces: self-similar capillary waves, and splashing as a new type of kinematic discontinuity, J. Fluid Mech. 283 (1995) 141–173.
[35] V.P. Carey, Liquid–Vapor Phase-Change Phenomena: An Introduction to the Thermophysics of Vaporization and Condensation Processes in Heat Transfer Equipment, in: G.F. Hewitt, C.L. Tien (Eds.), Series in Chemical and Mechanical Engineering, Taylor & Francis Series, Hemisphere, Washington, DC, 1992, p. xvii, 645.
[36] W.H. Zhuang, K. Etemadi, D.M. Benenson, N. Ashgriz, Sensitivity of the spreading rate of a liquid droplet on a surface to the approximation of the contact angle, Int. J. Model. Simul. 19 (2) (1999) 184–193.
[37] S.N. Reznik, A.L. Yarin, Spreading of an axisymmetric viscous drop due to gravity and capillarity on a dry horizontal wall, Int. J. Multiphase Flow 28 (9) (2002) 1437–1457.
[38] C.D. Stow, M.G. Hadfield, An experimental investigation of fluid flow resulting from the impact of a water drop with an unyielding dry surface, Proc. Roy. Soc. London Ser. A Math. Phys. Sci. 373 (1755) (1981) 419–441.
[39] P.V. Hobbs, Osheroff, Splashing of drops on shallow liquids, Science 158 (3805) (1967) 1184–1186.
[40] J. Shin, T.A. McMahon, The tuning of a splash, Phys. Fluids 2 (8) (1990) 1312–1317.
[41] G.E. Cossali, A. Coghe, M. Marengo, The impact of a single drop on a wetted solid surface, Exp. Fluids 22 (6) (1997) 463–472.
[42] C. Mundo, M. Sommerfeld, C. Tropea, Droplet-wall collisions: experimental studies of the deformation and breakup process, Int. J. Multiphase Flow 21 (2) (1995) 151–173.
[43] Photron USA Inc., www.photron.com, San Diego, CA; Distributed by Motion Engineering Company, www.motionengineering.com, Indianapolis, IN.
[44] J.D. Killion, Masters Thesis: An Investigation of Droplets and Films Falling over Horizontal Tubes, Department of Mechanical Engineering, Iowa State University, Ames, IA, 2003, p. 156.
[45] J.C. Russ, The Image Processing Handbook, CRC Press, Boca Raton, FL, 2002, p. 732.
[46] The Mathworks Inc., Matlab Version 6.5.0.180913a Release 13, Natick, MA, 2002. Available from <http://www.mathworks.com>.
[47] J. Canny, A computational approach to edge detection, IEEE Trans. Pattern Anal. Mach. Intell. PAMI-8 (6) (1986) 679–698.
[48] I.E. Sobel, Doctoral Thesis: Camera Models and Machine Perception, Dept. of Electrical Engineering, Stanford University, Palo Alto, 1970, p. 89 (also in Stanford Computer Science Dept. Artificial Intelligence Laboratory. AIM-121 technical report).
[49] C. de Boor, A Practical Guide to Splines, in: F. John et al. (Eds.), Applied Mathematical Sciences, Springer-Verlag, New York, 1978, p. xxiv, 392.
[50] E. Cohen, R.F. Riesenfeld, G. Elber, Geometric Modeling with Splines: An Introduction, AK Peters, Natick, MA, 2001, p. xxii, 616 p.
[51] The Mathworks Inc., Matlab Spline Toolbox, Ver. 3.1.1, Matlab Version 6.5.0.180913a Release 13, Natick, MA, 2002.
[52] W. Gander, W. Gautschi, Adaptive Quadrature—Revisited, BIT, vol. 40, 2000, pp. 84–101. Available from <http://www.inf.ethz.ch/personal/gander>.